Chemical Physics Letters 683 (2017) 160–165

Contents lists available at ScienceDirect

Chemical Physics Letters

journal homepage: www.elsevier.com/locate/cplett

Research paper

Ultrafast electron diffraction study of single-crystal $(EDO\text{-}TTF)_2SbF_6$: Counterion effect and dimensionality reduction

Lai Chung Liu [a,1], Yifeng Jiang [a,b,1], Henrike M. Mueller-Werkmeister [a,b], Cheng Lu [a], Gustavo Moriena [a], Manabu Ishikawa [c], Yoshiaki Nakano [c,d], Hideki Yamochi [c,d], R.J. Dwayne Miller [a,b,*]

[a] Department of Chemistry, University of Toronto, 80 St. George St, Toronto M5S 3H6, Canada
[b] Max Planck Institute for the Structure and Dynamics of Matter, Luruper Chaussee 149, 22761 Hamburg, Germany
[c] Research Centre for Low Temperature and Materials Sciences, Kyoto University, Sakyo-ku, Kyoto 606-8501, Japan
[d] Division of Chemistry, Graduate School of Science, Kyoto University, Sakyo-ku, Kyoto 606-8502, Japan

ARTICLE INFO

Article history:
Received 24 February 2017
In final form 2 May 2017
Available online 4 May 2017

Keywords:
Ultrafast electron diffraction
Femtosecond structural dynamics
Photoinduced phase transition
Singular value decomposition
Dimensionality reduction

ABSTRACT

Ultrafast electron diffraction is a sensitive tool to directly study molecular dynamics in structural detail. Here, we report the influence of counterion size on the photoinduced insulator-to-metal phase transition in two derivatives of the organic salt $(EDO\text{-}TTF)_2XF_6$. For X = P, three dominant motions are present and the molecules undergo the transition, whereas in the case of X = Sb, only two dominant motions are found and the molecules do not evolve into the metallic state. This reduction in dimensionality is supported by a novel data analysis method involving singular value decomposition of time-resolved electron diffraction data in reciprocal space.

1. Introduction

Molecular conductors—materials in which electrical conductivity is conferred by high charge mobility between the molecules—have been thoroughly studied from the viewpoints not only of potential industrial applications [1–4], but also of curiosity-driven sciences [5,6]. Among them, strongly correlated electron systems are of interest. The materials near the equilibrium lines of their phase diagram can undergo the phase transition when subjected to weak perturbations like changes in temperature and pressure [2,5,6]. In general, the insulator-to-metal (I–M) transition of molecular conductors is interpreted through some collective mechanisms such as Peierls distortion, charge-ordering (CO), order-disorder (OD), spin-density wave, and Mott transition [7–9].

Among strongly-correlated systems, the isostructural family of $(EDO\text{-}TTF)_2XF_6$, where EDO-TTF is 4,5-ethylenedioxytetrathiafulvalene and X is a pnictogen (P, As, and Sb), displays an I–M transition. Below the I–M transition temperature $T_{I\text{–}M}$, $(EDO\text{-}TTF)_2XF_6$ is in the insulator 'low temperature' (LT) phase, where charge is localized on the electron-donating EDO-TTF cations (D) in regular fashion along a stacking axis, represented by $(D^{+1}D^{+0}D^{+0}D^{+1})$; the electron-accepting XF_6 anions form sheets that separate these stacks. Various collective phenomena [10–16] cause periodic distortion along these donor columns, where the neutral molecules are bent and the charged ones remain flat. Above $T_{I\text{–}M}$, the charge delocalization occurs along the donor stacking direction, leading to a $(D^{+0.5}D^{+0.5}D^{+0.5}D^{+0.5})$ distribution within the crystal structure (shown in Fig. 1) and the onset of metallic properties. The transition mechanism is claimed to be the simultaneous manifestation of CO, OD, and Peierls distortion. Due to the multi-instability [13,14] of the metallic 'high temperature' (HT) phase, there is great interest in understanding the lattice relaxation processes that lead to these significant changes in material properties in undergoing these phase transitions.

In fact, in the case of X = P, it was found that the I–M phase transition can be triggered by photoexcitation using time-resolved vibrational spectroscopy and other transient spectroscopic techniques [11,12,15,17]. Optical pumping of the charge-transfer band leads to the formation of short-lived charge-ordered intermediate states and subsequent evolution to the HT metallic state [12]. Earlier work using ultrafast electron diffraction (UED) studied the structural dynamics of this photoinduced process with an instrument response function time of 430 fs within achievable signal-to-noise ratios [18]. Refinement of the diffraction data produced a 'molecular movie' that showcased the formation of a transient

* Corresponding author at: Department of Chemistry, University of Toronto, 80 St. George St, Toronto M5S 3H6, Canada (R.J.D. Miller).
E-mail address: dwayne.miller@mpsd.mpg.de (R.J.D. Miller).
[1] These authors contributed equally on this work.

http://dx.doi.org/10.1016/j.cplett.2017.05.007
0009-2614/

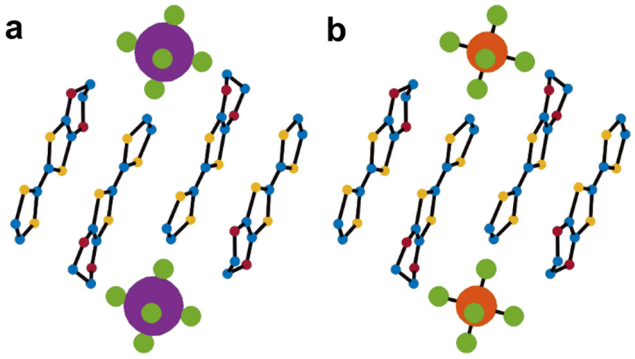

Fig. 1. Crystal structures as determined from X-ray diffraction at $T = 300$ K; (a) for $(EDO\text{-}TTF)_2SbF_6$ and (b) for $(EDO\text{-}TTF)_2PF_6$. In this view, the column of electron-donating EDO-TTF moieties is aligned with the horizontal axis.

intermediate state (INT) through the activation of three molecular modes. Correlation between the motion of the EDO-TTF and PF_6 molecules led to the conclusion that the PF_6 counterion plays a critical role in enabling the I–M phase transition by allowing the cations to approach each other and interact. Recent time-resolved optical reflectivity measurements on the SbF_6 derivative discovered that the anion substitution disabled the photoinduced formation of the metallic state [19]. The suggested mechanism was that the negative pressure from the larger counterion reduced the coupling between the EDO-TTF molecules by increasing the inter-stack distance and thus decreasing the coupling between donor molecules across the stacking axis.

We were motivated by the lack of direct structural confirmation of this counterion effect. Here, we follow up on the previous UED work in $(EDO\text{-}TTF)_2PF_6$ with a comparative study of the SbF_6 derivative to unravel the influence of counterion size on the ultrafast dynamics of this family of molecules. In particular, we adopt a novel data analysis approach by considering the similarity between broadband transient absorption spectra [20] and time-resolved electron diffraction data. We apply singular value decomposition (SVD) and global analysis to our UED intensities—newly measured for SbF_6 and previously published for PF_6 [18]—to successfully extract the principal components that underlie the structural dynamics of both $(EDO\text{-}TTF)_2SbF_6$ and $(EDO\text{-}TTF)_2PF_6$. By comparing the nature and timing of these key modes, we elucidate the role of the counterions in the lattice relaxation process leading to the photoinduced I–M phase transition.

2. Methods

Single crystals of $(EDO\text{-}TTF)_2SbF_6$ are prepared by electrocrystallization in ethanol; freshly purified $(Bu_4N)SbF_6$ is employed as the supporting electrolyte, while the original method used $(EMI)SbF_6$, where EMI denotes 1-ethyl-3-methylimidazolium [21]. These are cleaved by ultramicrotomy to a thickness of 150 nm. The resulting samples have typical sizes of 500 μm × 500 μm × 150 nm, which is optimal for UED in transmission mode at 95 keV. During the experiments, they are kept at 180 K, below the transition temperature of $(EDO\text{-}TTF)_2SbF_6$ ($T_{I-M} = 242$) [22]. This temperature ensures that the samples are fully in the LT insulator phase despite the large thermal hysteresis of 22 K [19].

UED is a pump-probe measurement; it uses femtosecond laser pulses to 'pump' the sample and femtosecond electron pulses to 'probe' for ultrafast structural changes [18,25–37]. In this work, a 95 keV DC-RF hybrid electron source [18,23] is used to probe the photoinduced dynamics of $(EDO\text{-}TTF)_2SbF_6$. The electron pulse duration is ~300 fs FWHM [24]. Due to the high brightness of the electron pulses, high quality time-resolved diffraction patterns are obtained even at the very low repetition rate of 10 Hz. This is done to avoid damage caused by cumulative heating from the pump laser pulses. The 60 fs pump laser pulses are centered at 800 nm and their polarization is adjusted to maximize the sample absorption via the charge transfer band. At the sample position, the pump laser has a pulse energy of 6.5 μJ and a diameter of 650 μm FWHM. The incident excitation fluence is 0.63 mJ/cm^2 and the excitation fraction is determined to be ~10%, using methods established in earlier UED work [18].

3. Results and discussions

The panels of Fig. 2 show electron diffraction patterns of the $(EDO\text{-}TTF)_2SbF_6$ samples under different static thermal and time-resolved photoinduced states. In Fig. 2a, the LT diffraction pattern recorded at 170 K is shown. A large number of Bragg spots can be seen, ranging from those close to the (000) transmitted beam to the high-order peaks near the edge of the camera sensor. This is evidence of the high crystallinity of the sample. In addition, the quality of the diffraction patterns demonstrates that the transverse coherence of the electron source is sufficiently large (estimated to be a few nanometres) to capture the structural changes. In Fig. 2b, the difference image between the LT data and that collected when the sample is in the HT state ($T = 300$ K) is shown. Red and blue patches indicate peaks which have respectively increased and decreased in intensity, and/or have shifted in position within reciprocal space. The former is associated with atomic displacements within the unit cell, while the latter is caused by changes in the shape and size of the unit cell. Using previously refined X-ray

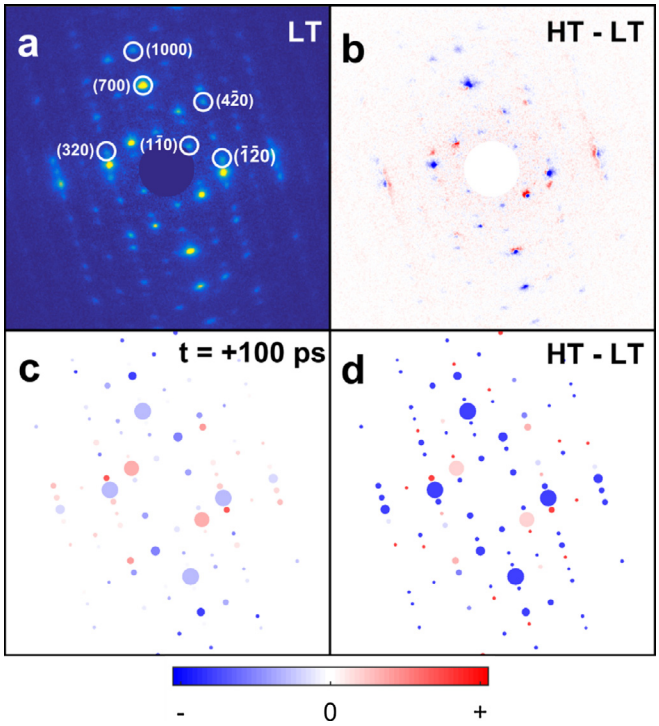

Fig. 2. Results of the UED experiment on $(EDO\text{-}TTF)_2SbF_6$: (a) the diffraction pattern of the sample in the LT state ($T = 170$ K), with a select number of peaks circled for later reference; (b) the difference diffraction pattern between the metallic HT state ($T = 300$ K) and the insulating LT state ($T = 170$ K); (c) the relative change in diffraction intensity 100 ps after photoexcitation; (d) integrated intensity data extracted from panel b for comparison with panel (c). Panels (c) and (d) are scatter plots of the main features of the respective diffraction patterns, where the marker position is determined by the position of the peaks, the marker size is scaled with the intensity of the peaks, and the marker fill colour is scaled with the change in peak intensity.

crystal structures, we found that these observed changes are consistent with the volume expansion and the structural reorganization correlated with the I–M phase transition of $(EDO\text{-}TTF)_2SbF_6$. In Fig. 2c and d, we show two 'reconstructed' diffraction patterns where each circle is sized according to the LT diffraction peak intensity, and coloured based on the relative change in intensity. The peak position is found by fitting to a two-dimensional Gaussian function and the peak intensity is calculated by integrating detector pixel intensities in a circular region around the peak centre. Fig. 2c shows the change in peak intensity 100 ps after photoexcitation and Fig. 2d plots the change in peak intensity caused by the thermal phase transition. A one-to-one comparison of the two patterns shows dissimilar intensity changes. This indicates that the late-time structure of the photoinduced state is different from that of the HT state. Furthermore, there was no discernible change in the fitted peak positions of the ground and photoexcited states. As discussed in Ref. 18, this is expected since the peak shifts associated with the photoinduced distortion of the $(EDO\text{-}TTF)_2XF_6$ unit cell are too small to be resolvable herein.

Fig. 3a and b show the temporal evolution of the relative change in diffraction intensity for a number of peaks measured for $(EDO\text{-}TTF)_2SbF_6$ and $(EDO\text{-}TTF)_2PF_6$, respectively. These were selected to highlight the diversity of signal contributions among the several hundred Bragg spots. Here, we observe clear differences in behaviour between the two EDO-TTF derivatives. While the PF_6 data is characterized by an 'ultrafast' sub-ps peak that is followed by a few-ps intermediate plateau and an exponential relaxation to a final state, the SbF_6 data only shows 'slow' (multi-ps) dynamics.

Previous analysis of UED data would involve a mapping from reciprocal to real space by building a structure model with which the diffraction pattern at each time point is refined against as a reference to get a set of time-dependent reaction coordinates. Instead, we consider a novel approach in which the structural dynamics are elucidated within reciprocal space directly. This approach provides a tractable mathematical analysis to project out the main structural changes since the number of observable Bragg spots (~200 Friedel pairs) is greater than the possible number of degrees of freedom (DOFs) available to $(EDO\text{-}TTF)_2XF_6$ ($N = 35$ non-H atoms in the asymmetric unit, $3N-6 = 99$ DOFs). This situation is analogous to the case of broadband transient absorption spectroscopy, where the number of sampled wavelengths is much larger than the number of optically active species within the probe volume. Thus, we apply singular value decomposition to reduce the amount of redundant complexity within our UED dataset. Redundant complexity refers to oversampling in reciprocal space; SVD is a generalization of eigenvalue decomposition to any $m \times n$ matrix, where

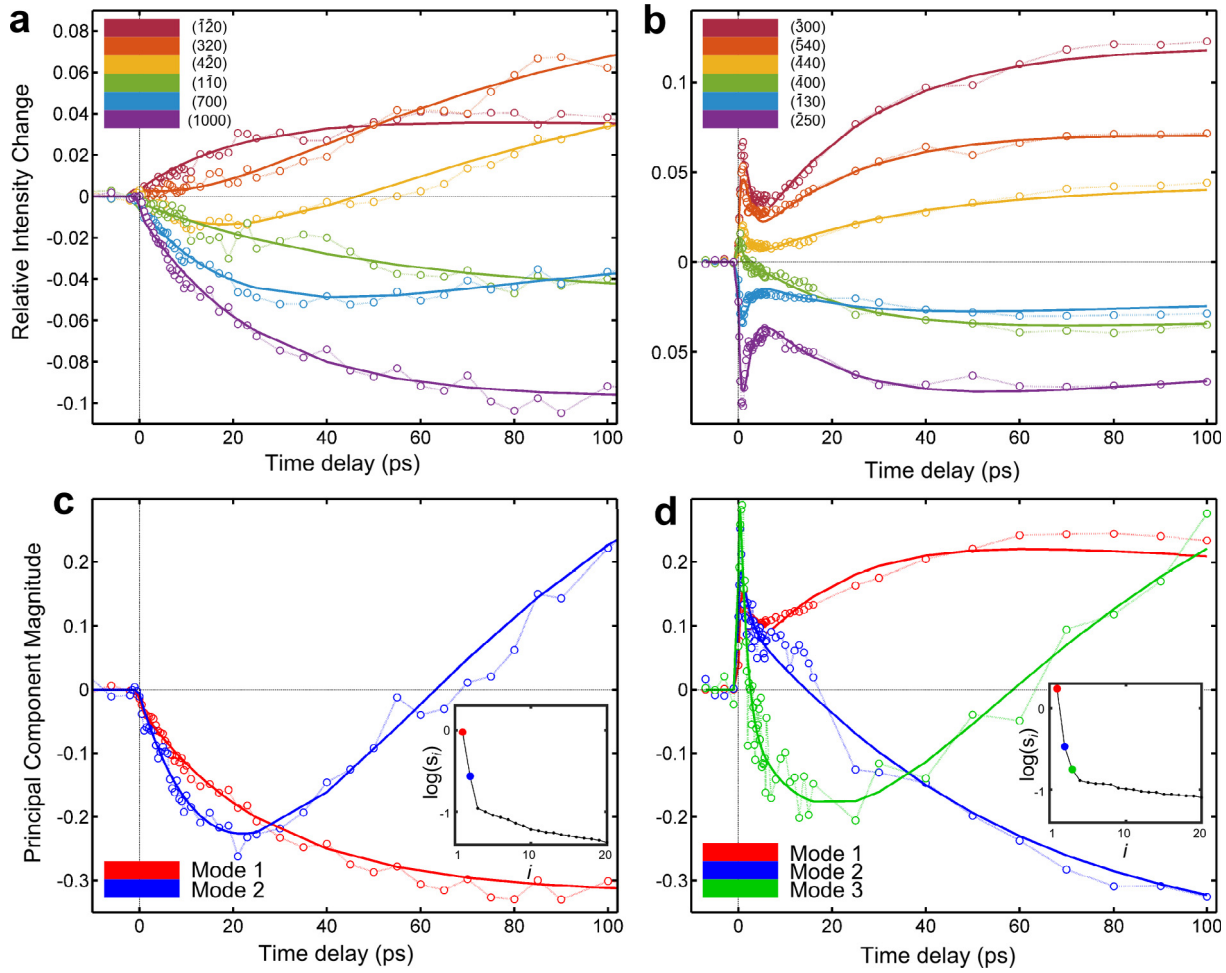

Fig. 3. Comparison of UED results for the two derivatives of $(EDO\text{-}TTF)_2XF_6$. The left two panels, (a) and (c), show results of X = Sb. The right two panels, (b) and (d), show comparable results of X = P. The top two panels, (a) and (b), show the relative change in the intensity of select diffraction peaks after photoexcitation; the thin lines with open circles are the experimental values while the thick solid lines are calculated from the fitted results in the bottom panels. The bottom two panels, (c) and (d), show the results of the SVD analysis; the thin lines with open circles in the main panels are the major right-singular vectors; the thick solid lines are the global exponential fits of these vectors; the insets are plots of the logarithm of the singular values as a function of their matrix index. These comparisons highlight the dramatic difference in structural dynamics with the change in counterion.

it is factorized into three parts: a $m \times n$ diagonal matrix (with 'singular values' along the diagonal) bracketed by $m \times m$ left and $n \times n$ right unitary matrices (whose columns are the left- and right- 'singular vectors' respectively) [38].

In our SVD analysis, the UED intensity change dataset is concatenated into an $N_k \times N_t$ matrix, where N_k is the number of Bragg spots (i.e., k-points) and N_t, the number of time delay points. Others have proposed a similar method where SVD is applied in real space to electron density maps roughly refined from time-resolved X-ray crystallographic data [39]. By effectively diagonalizing the UED data matrix, SVD yields an orthogonal basis set that fully spans the sampled spaces: the left-singular vectors for the reciprocal space domain and the right-singular vectors for the time domains. Since reciprocal space is dual to real space, the left-singular vectors simply represents orthogonal sets of atomic motions. Furthermore, we find that all but the first few singular values are effectively zero. As seen in the insets of Fig. 3c and d, there is a clear point of flexion in the logarithmic plot of the singular values over matrix indices. The singular values above this point of flexion coincide with right-singular column vectors whose values for $t > 0$ ps are significantly larger than those for $t < 0$ ps, while for those below, the equivalent vectors show no discernible photo-triggered signal. We refer to these vectors as the principal components of the dataset; they are plotted for the case of the SbF_6 and PF_6 derivatives as thin lines in Fig. 3c and d. A global analysis model based on a sum of exponential terms is used to fit these principal components and the results are shown as thick solid lines in Fig. 3c and d. No decay- or species-associated analysis is performed since UED probes structural distortions of locally excited molecules, not uniquely associated populations of excited states which follow photochemical kinetics. In the SbF_6 case, only two principal components are necessary to describe the entire dataset. They are jointly fitted with two exponential terms with time constants $\tau_1 = 25.23$ ps and $\tau_2 = 51.65$ ps. In the PF_6 case, there are three principal components and four exponential terms are needed to describe the dynamics, $\tau_1 = 0.99$ ps, $\tau_2 = 1.07$ ps, $\tau_3 = 28.01$ ps, $\tau_4 = 45.49$ ps.

Another insightful and independent approach to analysing UED data within reciprocal space is the Pearson correlation analysis. By calculating the Pearson correlation coefficient between the UED intensity of the photoexcited state at time t and the corresponding thermal equilibrium state T, $P_T(t) = \mathrm{cov}(I(t), I_T)/\sigma_t\sigma_T$, the trajectory of the excited state within the HT and LT configuration space is obtained as a line connecting the points $(P_{HT}(t), P_{LT}(t))$. In Fig. 4a and b, these results are shown. These values were normalized to ensure that the coordinates (1, 0) and (0, 1) represent perfect correlation with the HT and LT states, respectively. For $t < 0$ ps, the trajectory is at the LT ground state. After $t = 0$ ps, the molecules are photoexcited and the trajectory of the two derivatives diverge rapidly. In Fig. 4a, it can be seen that the $(EDO\text{-}TTF)_2SbF_6$ molecule evolves away from the ground LT state but not directly towards the HT state. This structural transformation occurs on a time scale on the order of tens of picoseconds and ends at a conformation that is unlike both LT and HT states. In Fig. 4b, the trajectory for the PF_6 derivative is shown. Upon photoexcitation, the molecule moves away from the ground LT state towards the HT state, overshoots the transient INT state, undergoes an overdamped half-cycle decay, remains stationary for a few ps at the INT state, then relaxes exponentially to the structure corresponding to the final HT state.

The clear difference in shape of these two conformation trajectories highlight the important role played by the counterion in the photoinduced I–M phase transition in $(EDO\text{-}TTF)_2XF_6$. Earlier UED work on the PF_6 derivative [18] identified the three independent correlated molecular motions that comprise the basis set for fully describing the overall structural dynamics; one of these three modes is the counterion motion. It concluded that the counterion motion is correlated with the formation of the transient INT state. Here, our analysis recovers these modes—sliding of flat EDO-TTF molecules, unbending of bent EDO-TTF molecules, and motion of PF_6 counterions—as the three principal components of the SVD results. Given that the SbF_6 trajectory avoids the equivalent INT region of the (P_{HT}, P_{LT})-conformation space, the missing SbF_6 principal component that would be expected from photoexcitation is the equivalent counterion motion. This absence of the key counterion

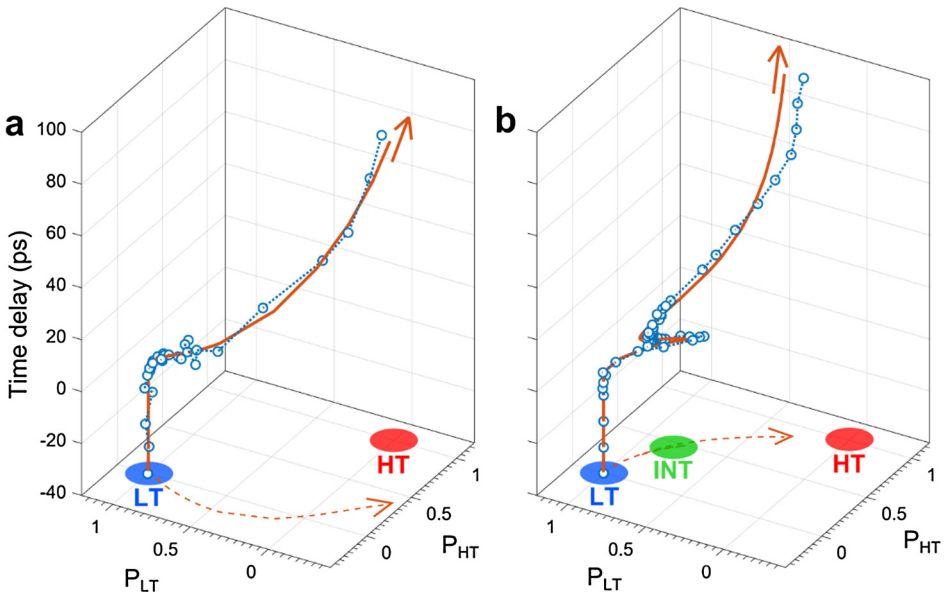

Fig. 4. The effect of counterion substitution on photoinduced structural dynamics. The two panels shows the time evolution of the Pearson correlation coefficient between the photoexcited structure and the thermal equilibrium structures (LT and HT) of $(EDO\text{-}TTF)_2XF_6$ (X = (a) Sb and (b) P). At each time delay, the similarity between the diffraction patterns is represented by the pair of values (P_{HT}, P_{LT}), where $P = 0$ means no correlation, and $P = 1$ perfect correlation. The blue dotted line with open circles is from the measured peak intensities; the solid orange line is from the fitted SVD-reduced peak intensities; the orange dashed line illustrates the trajectory of the photoexcited state projected onto the (HT, LT) configuration space, where the identifiable states are labeled. The atomic motions in the presence of the Sb counterion are clearly insufficient to allow the full relaxation to the spatial relationships consistent with the metallic state.

mode explains the deactivation of the photoinduced I–M pathway and is consistent with the proposed mechanism in an earlier spectroscopic study on $(EDO\text{-}TTF)_2SbF_6$ [19]. Although the counterions are not directly involved in the photophysics, they play a crucial role in passively directing structural reorganization of the photoexcited cations. This observation can be rationalized when one considers the change in the local electric field due the photoinduced electron transfer process between EDO-TTF moieties. The counterion motion in response to this reaction force is observed to be the largest and dominant motion that directs the lattice reorganization that destabilizes the charge ordered state. This motion is evidently intimately coupled to the collective lattice response and changes in material properties in going from one phase to another. Work in another photoactive system, $X[Pd(dmit)_2]_2$ ($X = Et_2Me_2Sb$ and Cs), also studied the effect of counterion size and indirectly found that the substitution for a larger counterion slowed and changed the mechanism of the photoinduced dynamics [40]. Our UED results offer the first direct structural evidence of the counterion effect on the lattice reorganization destabilizing the charge order and its role in the formation of the metallic state. The observations clearly show that there are only a few types of motion that dominate the structural transition, as opposed to equipartitioning of all possible motions. This process appears general and herein referred to as dimensionality reduction [41]. The notion of key reaction modes has been discussed in the field of chemistry for some time. We now can observe these motions directly and rationalize how even the simple change in counterion can affect both the degree of lattice reorganization to charge transfer processes and control macroscopic material properties. Further, we have successfully demonstrated here how SVD belongs in the standard tool box for interpreting time-resolved diffraction data directly without relying on a refinement model that maps reciprocal space to real space.

4. Conclusions

The present study is the first comparative UED study of an isostructural family of molecules with the goal of investigating the interplay between structural dynamics and molecular function in close detail. We choose two derivatives of the well-studied molecular system $(EDO\text{-}TTF)_2XF_6$, of which one (X = P) can undergo an insulator-to-metal phase transition under photoexcitation. From our results, we show that the size of the counterion is a key factor for determining the activity of the photoinduced I–M pathway and the dimensionality of associated structural dynamics. In the case of X = P, the atomic motions are three-dimensional in generalized coordinates, with three principal DOFs, where the counterion movement leads to lattice relaxation that supports the formation of the metallic state. When X is replaced with Sb, the structural dynamics becomes two-dimensional as the counterion is effectively too large to avoid hindering the interactions between the EDO-TTF moieties. This obstruction prevents full relaxation to structural relationships that enable sufficient charge redistribution and spatial electron delocalization, which lead to the formation of a metallic band structure. This conclusion is drawn without resorting to structural models but rather by the use of singular value decomposition in reciprocal space. This approach has been well-established for spectroscopic techniques for overlapping spectral components. Here, we use this as an unbiased approach to analyze diffraction data to project out the dominant motions involved in structural dynamics. There are clearly only a few key modes or types of motion involved, which greatly reduces the overall dimensionality of the problem in relation to the consideration of all possible nuclear motions convolved to a speculative reaction coordinate. The identification of these key modes in turn greatly simplifies the problem in terms of controlling molecular processes. These findings illustrate the great promise that this technique bears for further application to other diffraction experiments.

Acknowledgements

We thank Ryan L. Field, Meng Gao, Donald Kelloway, Stuart A. Hayes, Alexander Marx, and Herlander D. Pinto for helpful discussions; we also thank Alan J. Lough for performing preliminary X-ray diffraction on the samples. Funding for this work was provided by grants from the Canadian Institute for Advanced Research (CIFAR), the National Sciences and Engineering Research Council (NSERC), the People Programme (Marie Curie Actions) of the European Union's Seventh Framework Programme (FP7/2007-2013) under REA grant agreement no. 623994 (H. M.-W.), and Grants-in-Aid for Scientific Research (KAKENHI) grant no. JP15K17901, JP17H05153, and JP26288035 from the Japan Society for the Promotion of Science (JSPS). This work has been supported by the excellence cluster "The Hamburg Centre for Ultrafast Imaging - Structure, Dynamics and Control of Matter at the Atomic Scale" of the Deutsche Forschungsgemeinschaft and by the Max Planck Society. We declare no conflict of interest.

References

[1] K.P. Goetz et al., Charge-transfer complexes: new perspectives on an old class of compounds, J. Mater. Chem. C 2 (2014) 3065–3076.
[2] T. Mori, Principles that govern electronic transport in organic conductors and transistors, Bull. Chem. Soc. Jpn. 89 (2016) 973–986.
[3] S. Hotta et al., Organic single-crystal light-emitting field-effect transistors, J. Mater. Chem. C 2 (2014) 965–980.
[4] W. Brütting & C. Adachi (ed). Physics of organic semiconductors. Edn. 2. (Wiley-VCH Verlag GmbH & Co. KGaA, Weinheim, Germany, 2005). https://dx.doi.org/10.1002%2F9783527654949.
[5] J. Fraxedas, Molecular organic materials from molecules to crystalline solids, Cambridge University Press, 2008, http://dx.doi.org/10.1017/cbo9780511525216.
[6] A. Gabovich (Ed.), Superconductors – materials, properties and applications, InTech, Rijeka, Croatia, 2012, http://dx.doi.org/10.5772/2577.
[7] T. Isiguro, K. Yamaji, G. Saito, Organic superconductors. Edn. 2. (Springer-Verlag, Berlin/Heidelberg, Germany, 1998). https://dx.doi.org/10.1007/978-3-642-58262-2.
[8] B. Köhler et al., Comprehensive transport study of anisotropy and ordering phenomena in quasi-one-dimensional $(TMTTF)_2X$ salts ($X = PF_6$, AsF_6, SbF_6, BF_4, ClO_4, ReO_4), Phys. Rev. B 84 (2011) 035124.
[9] J.-P. Pouget, Interplay between electrical and structural degrees of freedom in quarter-filled low dimensional conductors, Phys. B 460 (2015) 45–52.
[10] M. Filatov, Antiferromagnetic interactions in the quarter-filled organic conductor $(EDO\text{-}TTF)_2PF_6$, Phys. Chem. Chem. Phys. 13 (2011) 12328–12334.
[11] K. Onda et al., Photoinduced change in the charge order pattern in the quarter-filled organic conductor $(EDO\text{-}TTF)_2PF_6$ with a strong electron-phonon interaction, Phys. Rev. Lett. 101 (2008) 067403.
[12] K. Iwano, Y. Shimoi, Large electric-potential bias in an EDO-TTF tetramer as a major mechanism of charge ordering observed in its PF_6 salt: a density functional theory study, Phys. Rev. B 77 (2008) 075120.
[13] H. Yamochi, S.-Y. Koshihara, Organic metal $(EDO\text{-}TTF)_2PF_6$ with multi-instability, Sci. Technol. Adv. Mater. 10 (2009) 024305.
[14] K. Onda, H. Yamochi, S.-Y. Koshihara, Diverse photoinduced dynamics in an organic charge-transfer complex having strong electron-phonon interactions, Acc. Chem. Res. 47 (2014) 3494–3503.
[15] A. Ota, H. Yamochi, G. Saito, A novel metal–insulator phase transition observed in $(EDO\text{-}TTF)_2PF_6$, J. Mater. Chem. 12 (2002) 2600–2602.
[16] M. Tsuchiizu, Y. Suzumura, Peierls ground state and excitations in the electron-lattice correlated system $(EDO\text{-}TTF)_2X$, Phys. Rev. B 77 (2008) 195128.
[17] N. Fukazawa et al., Charge and structural dynamics in photoinduced phase transition of $(EDO\text{-}TTF)_2PF_6$ examined by picosecond time-resolved vibrational spectroscopy, J. Phys. Chem. C 116 (2012) 5892–5899.
[18] M. Gao et al., Mapping molecular motions leading to charge delocalization with ultrabright electrons, Nature 496 (2013) 343–346.
[19] M. Servol et al., Local response to light excitation in the charge-ordered phase of $(EDO\text{-}TTF)_2SbF_6$, Phys. Rev. B 92 (2015) 024304.
[20] R. Field et al., Spectral signatures of ultrafast spin crossover in single crystal $[Fe^{II}(bpy)_3](PF_6)_2$, Chem. Eur. J. 22 (2016) 1521–3765, http://dx.doi.org/10.1002/chem.201600374.

[21] M. Maesato et al., Control of metal-insulator transition in (EDO-TTF)$_2$SbF$_6$, J. Phys. Conf. Ser. 148 (2009), http://dx.doi.org/10.1088/1742-6596/148/1/012004, 012004.
[22] Y. Nakano et al., Anion size and isotope effects in (EDO-TTF)$_2$SF$_6$, J. Phys. Conf. Ser. 148 (2009) 012007.
[23] M. Gao et al., Full characterization of RF compressed femtosecond electron pulses using ponderomotive scattering, Opt. Express 20 (2012) 12048–12058.
[24] M. Gao et al., Single shot time stamping of ultrabright radio frequency compressed electron pulses, Appl. Phys. Lett. 103 (2013) 033503.
[25] H. Ihee et al., Direct imaging of transient molecular structures with ultrafast electron diffraction, Science 291 (2001) 458–462.
[26] B.J. Siwick et al., An atomic-level view of melting using femtosecond electron diffraction, Science 302 (2003) 1382–1385.
[27] C.-Y. Ruan et al., Ultrafast electron crystallography of interfacial water, Science 304 (2004) 80–84.
[28] S. Nie et al., Measurements of the electronic Grüneisen constant using femtosecond electron diffraction, Phys. Rev. Lett. 96 (2006), http://dx.doi.org/10.1103/physrevlett.96.025901, 025901.
[29] P. Baum, D.-S. Yang, A.H. Zewail, 4D visualization of transitional structures in phase transformations by electron diffraction, Science 318 (2007) 788–792.
[30] G. Sciaini et al., Electronic acceleration of atomic motions and disordering in bismuth, Nature 458 (2009) 56–59.
[31] T. van Oudheusden et al., Compression of subrelativistic space-charge-dominated electron bunches for single-shot femtosecond electron diffraction, Phys. Rev. Lett. 105 (2010) 2648901, http://dx.doi.org/10.1103/physrevlett.105.264801.
[32] H. Jean-Ruel et al., Ring-closing reaction in diarylethene captured by femtosecond electron crystallography, J. Phys. Chem. B 117 (2013) 15894–15902.
[33] M. Eichberger et al., Snapshots of cooperative atomic motions in the optical suppression of charge density waves, Nature 468 (2010) 799–802, http://dx.doi.org/10.1038/nature09539.
[34] M. Hada et al., Cold ablation driven by localised forces in alkali halides, Nat. Comm. 5 (2014) 3863, http://dx.doi.org/10.1038/ncomms4863.
[35] R.P. Chatelain et al., Coherent and incoherent electron-phonon coupling in graphite observed with radio-frequency compressed electron diffraction, Phys. Rev. Lett. 113 (2014) 235502.
[36] T. Ishikawa et al., Direct observation of collective modes coupled to molecular orbital-driven charge transfer, Science 350 (2015) 1501–1505.
[37] L. Waldecker et al., Time-domain separation of optical properties from structural transitions in resonantly bonded materials, Nat. Mat. 14 (2015) 991–995.
[38] L.J.G.W. van Wilderen, C.N. Lincoln, J.J. van Thor, Modeling multi-pulse population dynamics from ultrafast spectroscopy, PLoS ONE 6 (2011) e17373.
[39] M. Schmidt et al., Application of singular value decomposition to the analysis of time-resolved macromolecular X-ray data, Biophys. J. 84 (2003) 2112–2129.
[40] N. Fukazawa et al., Time-resolved infrared vibrational spectroscopy of the photoinduced phase transition of Pd(dmit)$_2$ salts having different orders of phase transition, J. Phys. Chem. C 117 (2013) 13187–13196.
[41] R.J.D. Miller, Ultrafast imaging of photochemical dynamics: roadmap to a new conceptual basis for chemistry, Faraday. Discuss. 194 (2016) 777–828.